Mendeleev Communications

Mendeleev Commun., 2025, **35**, 327–330

Impact of fluorination on optoelectronic properties of thiophene-benzothiadiazole-based hole-transport polymers for perovskite solar cells

Ekaterina A. Komissarova,*[a] Sergei A. Kuklin,[a,b] Nikita A. Slesarenko,[a] Alina F. Latypova,[a] Azat F. Akbulatov,[a] Victoria V. Ozerova,[a] Maria N. Kevreva,[a] Nikita A. Emelianov,[a] Lyubov A. Frolova[a] and Pavel A. Troshin[c,a]

[a] *Federal Research Center of Problems of Chemical Physics and Medicinal Chemistry, Russian Academy of Sciences, 142432 Chernogolovka, Moscow Region, Russian Federation. E-mail: ekaterina.komva@inbox.ru*
[b] *A. N. Nesmeyanov Institute of Organoelement Compounds, Russian Academy of Sciences, 119334 Moscow, Russian Federation*
[c] *Zhengzhou Research Institute of HIT, Jinshui District, 450003 Zhengzhou, China*

DOI: 10.71267/mencom.7632

Novel polymers composed of thiophene units combined with non-fluorinated and fluorinated 2,1,3-benzothiadiazole units were synthesized and investigated as hole transport materials in perovskite solar cells. The impact of backbone fluorination on the optical and electronic properties of the resulting materials as well as the nanoscale morphology of their films deposited on the perovskite absorber layer was elucidated. The fluorinated polymer provided a superior power conversion efficiency of 18.6% coupled with high open-circuit voltage (V_{OC} = 1.047 V) and short-circuit current (J_{SC} = 23.4 mA cm^{-2}).

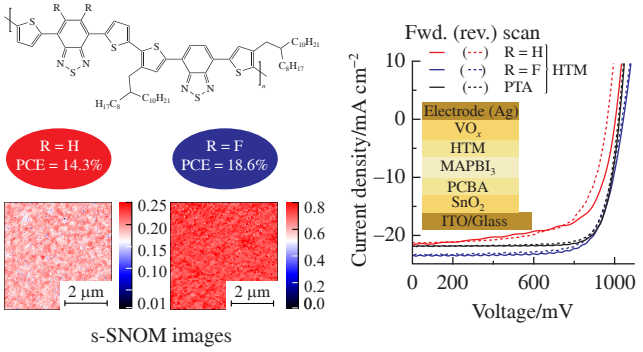

Keywords: thiophene, 2,1,3-benzothiadiazole, Stille cross-coupling, IR s-SNOM, hole transport materials, perovskite solar cells, PSCs.

Perovskite solar cells (PSCs) are one of the most promising emerging photovoltaic technologies. The power conversion efficiency (PCE) of PSCs has reached >26%, which is close to that of crystalline silicon solar cells, demonstrating the great potential of PSCs technology.[1,2] To achieve high efficiency and stability of PSCs, it is necessary to ensure the matching of energy levels of charge transfer interlayers and perovskite absorber material, as well as uniformity and low defect concentration in the charge transport layers. From this point of view, organic π-conjugated polymers are considered as promising hole transport materials (HTMs) for PSCs.[3]

Organic conjugated donor–acceptor polymers can serve as dopant-free HTMs for the fabrication of efficient and stable PSCs due to their inherent advantages such as tunable frontier orbital energy levels, chemical and thermal stability and good carrier mobility.[4–9] The introduction of fluorine atoms into the polymer backbone is an effective approach to optimize the optoelectronic properties of conjugated polymers by lowering the frontier orbital energy.[10–15] In addition, fluorine atoms promote the planar configuration of the polymer backbone, which results in their favorable packing in thin films and a more pronounced tendency to aggregate when going from solutions to thin films compared to their fluorine-free counterparts.[16] Note that 2,1,3-benzothiadiazole is an actively used fragment for organic semiconductor materials due to its planar and rigid geometry, heteroatom interactions, high absorption coefficient, electrochemical stability and electron-withdrawing ability.[17]

In this communication, we report the synthesis of two new polymers whose molecular structures consist of alternating thiophene and benzothiadiazole moieties. We have particularly focused on investigating the effect of introducing fluorine atoms into the polymer backbone on the optoelectronic properties of the designed materials and their performance as HTMs in PSCs. The aim of this work was to evaluate the potential of the molecular design strategy involving the introduction of fluorine substituents in the context of further rational development of promising materials for high-efficiency PSCs.

Conjugated polymers **P1** and **P2** were synthesized *via* a palladium-catalyzed Stille polycondensation reaction using monomers **M1** and **M2**, respectively, in combination with monomer **M3** (Scheme 1). Detailed syntheses of key monomers and polymers **P1** and **P2** are provided in Online Supplementary Materials.

The resulting polymers were precipitated with methanol and purified by a series of Soxhlet extractions with acetone, hexane, dichloromethane, chlorobenzene and finally 1,2-dichlorobenzene. The polymer fractions extracted with the last two solvents were collected, concentrated *in vacuo* and then precipitated with acetone. Dynamic gel permeation chromatography was used to analyze the relative molecular weight characteristics of polymers **P1** and **P2** (Table 1). Polymer **P2** showed a lower molecular weight than polymer **P1**, presumably due to strong intermolecular aggregation resulting in decreased solubility and precipitation from the reaction mixture starting at the lower molecular weight.

The thermal properties of the conjugated polymers were studied by thermogravimetric analysis under nitrogen atmosphere at a heating rate of 10 °C min^{-1}. The thermogravimetric curves are shown in Figure S5 (see Online Supplementary Materials) and the results are listed in Table 1. The decomposition temperatures (T_d, at 5% weight loss) for polymers **P1** and **P2** were around 414 °C, indicating good thermal stability of these polymers.

The optical properties of polymers **P1** and **P2** were investigated in solutions and thin films by UV-VIS spectroscopy [Figure 1(*a*),(*b*)]. Both polymers in 1,2-dichlorobenzene solution show two absorption

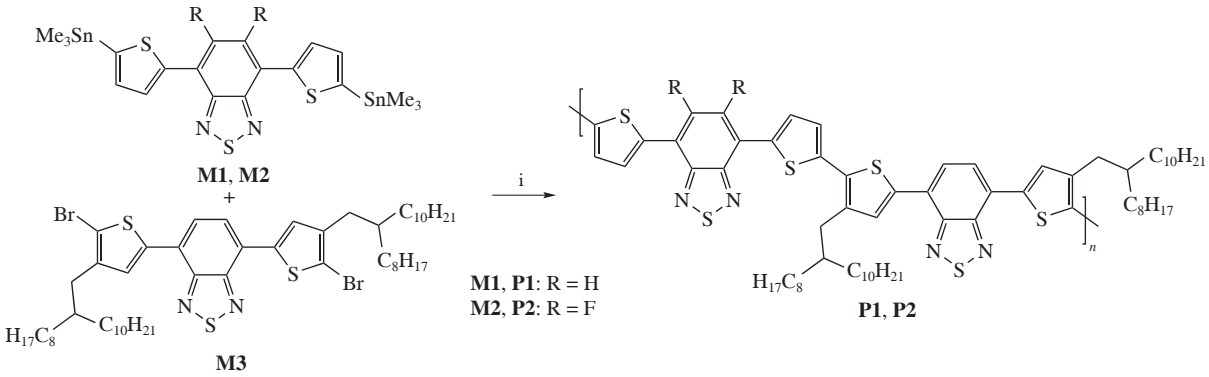

Scheme 1 *Reagents and conditions*: i, $Pd_2(dba)_3$, $(o\text{-}MeC_6H_4)_3P$, toluene.

Table 1 Physicochemical and optoelectronic properties of polymers **P1** and **P2**.

Polymer	M_w[a]/kDa	M_w/M_n[b]	T_d[c]/°C	λ_{max}^{sol} (λ_{max}^{film})[d]/nm	E_g^{opt}[e]/eV	PL_{max}[f]/nm	E_{onset}^{ox}[g]/V *vs.* Fc^+/Fc	HOMO (LUMO)[h]/eV
P1	165	1.19	414	406, 670, 740 (405, 662, 720)	1.60	802	0.31	−5.11 (−3.51)
P2	21	2.96	414	386, 600 (396, 635)	1.65	780	0.42	−5.22 (−3.57)

[a] Weight-average molecular weight. [b] Polydispersity index. [c] Decomposition temperature corresponding to 5% weight loss. [d] Absorption maxima of polymers in solution (thin film). [e] Optical energy band gap estimated using Tauc plots derived from absorption spectra of thin films. [f] Photoluminescence maxima of polymers in thin films. [g] Potential of oxidation wave onset. [h] HOMO energy estimated from CV measurements and LUMO energy estimated as E_g^{opt} + HOMO.

bands in the range of 400–800 nm [see Figure 1(*a*)]. The band near 400 nm can be attributed to the π–π* transition within the monomeric units of the polymer backbone, while the broader bands in the long-wavelength region of 600–750 nm are assigned to the intramolecular charge transfer interaction between the donor and acceptor units. The absorption band maxima of fluorinated polymer **P2** are blue-shifted compared to those of polymer **P1**. The absorption spectrum of the thin film of polymer **P1** shows minimal changes compared to that in solution. The spectra of polymer **P2** in solution and thin films show a shoulder at around 700 nm, indicating enhanced aggregation of macromolecules at room temperature. For fluorinated polymer **P2**, the absorption spectra of thin films show a slight bathochromic shift compared to solution, indicating additional aggregation in the solid state [see Figure 1(*b*)]. The optical band gaps (E_g^{opt}) of 1.60 and 1.65 eV for polymers **P1** and **P2**, respectively, were estimated from the Tauc plots [see Table 1 and Figure 1(*c*)]. The band gap of polymer **P1** is slightly smaller than that of its fluorinated counterpart **P2**. The photoluminescence (PL) band maxima of polymers **P1** and **P2** are located at 802 and 780 nm, respectively, which is consistent with the band gap values estimated from the absorption spectra [Figure 1(*d*)].

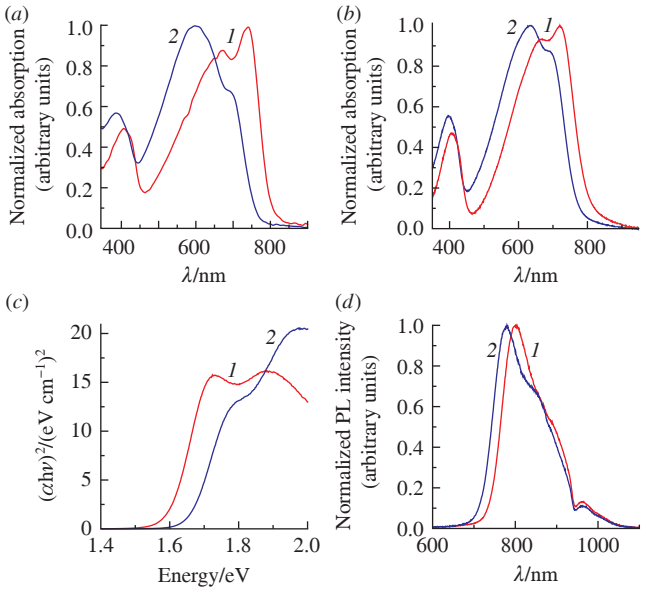

Figure 1 Optical properties of (*1*) polymer **P1** and (*2*) polymer **P2**: absorption spectra (*a*) in 1,2-dichlorobenzene solutions and (*b*) in thin films, (*c*) Tauc plots for thin films and (*d*) steady-state PL spectra in thin films.

The electrochemical properties of the polymers were investigated using cyclic voltammetry (CV) measurements and the obtained CV curves are shown in Figure S6. The energies of the highest occupied molecular orbital (HOMO) and the lowest unoccupied molecular orbital (LUMO) were estimated using the standard approach: $E_{HOMO} = -[E_{onset}^{ox}$ (*vs.* Fc^+/Fc) + 4.8]/eV[18] and $E_{LUMO} = E_g^{opt} + E_{HOMO}$/eV. The corresponding numeric data are summarized in Table 1. The HOMO and LUMO energy levels of the fluorinated polymer **P2** were slightly lower than those of the non-fluorinated polymer **P1** (see Table 1). The observed difference is apparently due to the presence of electron-withdrawing fluorine atoms in polymer **P2**.

The photovoltaic performance of polymers **P1** and **P2** as HTMs was investigated in PSCs fabricated in n-i-p architecture with the ITO/SnO_2/PCBA/$MAPbI_3$/HTM/VO_x/Ag structure [Figure S7(*a*)]. To passivate the surface defects on the SnO_2 layer, we deposited a phenyl-C_{61}-butyric acid (PCBA) layer [Figure S7(*b*)]. Poly[bis-(4-phenyl)(4-methylphenyl)amine] (PTA), which is commonly used in n-i-p PSCs, was used as a reference HTM [see Figure S7(*b*)]. Figure 2(*a*),(*b*) shows the current–voltage characteristics of the champion devices assembled with polymer **P1**, polymer **P2** and PTA as HTMs. The device parameters are summarized in Table 2.

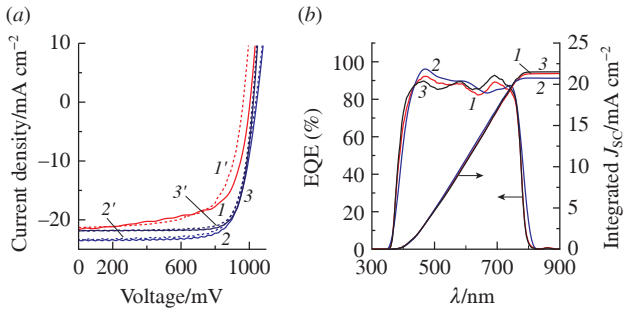

Figure 2 Photovoltaic performance of polymers **P1** and **P2** as HTMs in n-i-p PSCs: (*a*) current–voltage curves for (*1*)–(*3*) forward and (*1′*)–(*3′*) reverse scan directions and (*b*) EQE and short-circuit current density spectra of the PSCs using (*1*) polymer **P1**, (*2*) polymer **P2** and (*3*) PTA as HTMs.

Table 2 Characteristics of n-i-p PSCs fabricated using polymer **P1**, polymer **P2** and PTA as HTMs.

HTM	Scan direction	V_{OC}[a]/V	J_{SC}[b]/ mA cm^{-2}	FF[c] (%)	PCE[d] (%)
P1	Forward	1.004	21.7	66	14.3
	Reverse	0.964	21.3	67	13.8
P2	Forward	1.047	23.4	75	18.6
	Reverse	1.041	23.3	73	17.9
PTA	Forward	1.024	21.8	80	17.8
	Reverse	1.019	21.8	78	17.5

[a] Open-circuit voltage. [b] Short-circuit current density. [c] Fill factor. [d] Power conversion efficiency.

PSCs using fluorinated polymer **P2** as the HTM showed improved photovoltaic performance compared to devices fabricated with its non-fluorinated counterpart **P1**. Polymer **P2** provided higher open-circuit voltage (V_{OC} = 1.047 V) and short-circuit current density (J_{SC} = 23.4 mA cm^{-2}), resulting in a PCE of 18.6%, while non-fluorinated polymer **P1** delivered a PCE value just over 14% (see Table 2). Interestingly, this trend is in good agreement with the fact that the HOMO level of polymer **P2** is 0.11 eV closer to that of perovskite (−5.35 eV), which may reduce the potential barrier for charge carrier extraction from $MAPbI_3$ into the charge-transport layer. Devices with polymer **P2** as the HTM show slightly better photovoltaic performance than PTA under the same experimental conditions.

The morphology and uniformity of the polymer films deposited on the perovskite absorber layer are crucial for the efficient performance of the PSCs. We used atomic force microscopy (AFM) and infrared scattering-type scanning near-field optical microscopy (IR s-SNOM)[19] to visualize the morphology of the polymer films. Figure 3 shows the AFM scanning and IR s-SNOM mapping images of the perovskite/HTM stacks. In some areas of the scans, the $MAPbI_3$/polymer **P1**, $MAPbI_3$/polymer **P2** and $MAPbI_3$/PTA films show weak contrast, which is likely due to the surface topography of the perovskite layer revealed in the AFM images. Probably, in this case, the polymer films are thinner at the top of the perovskite grains. Therefore, a weak signal corresponding to the perovskite sublayer is visible. Scanning of the $MAPbI_3$/polymer **P1** samples revealed the presence of multiple point defects, which appear as blue spots [Figure 3(*b*)] and red spots [Figure 3(*c*)]. Such defects enable a direct contact of $MAPbI_3$ with VO_x and the top electrode, which negatively affects the efficiency and stability of the fabricated PSCs. In contrast, the $MAPbI_3$/polymer **P2** stacks exhibit a high degree of uniformity of the coatings formed by polymer **P2**. Thus, the remarkable difference in the uniformity of the films made of polymers **P1** and **P2** is most likely responsible for the drastically different photovoltaic performance of PSCs with these two polymers as hole-transport layer materials.

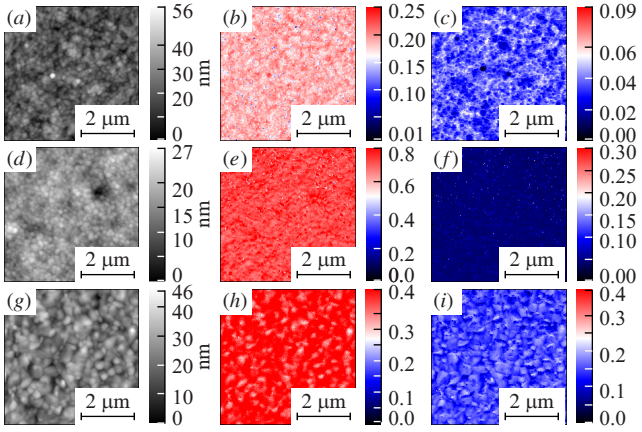

Figure 3 Morphology of (*a*)–(*c*) polymer **P1**, (*d*)–(*f*) polymer **P2** and (*g*)–(*i*) PTA films deposited on perovskite absorber films: (*a*),(*d*),(*g*) AFM topography images and IR s-SNOM mapping images at the characteristic frequencies of the IR absorption bands of (*b*) polymer **P1**, (*e*) polymer **P2**, (*h*) PTA and (*c*),(*f*),(*i*) $MAPbI_3$ perovskite.

In conclusion, we synthesized two novel $(TBT)_n$-type conjugated polymers **P1** and **P2**, consisting of thiophene blocks and non-fluorinated or fluorinated benzothiadiazole moieties, respectively. The introduction of fluorine atoms into the polymer backbone was found to have a strong influence on the physicochemical (particularly molecular weight and solubility), optical and electrochemical properties of the polymers. The obtained polymers were investigated as HTMs in PSCs. Devices assembled using the fluorinated polymer **P2** showed significantly improved photovoltaic performance compared to cells with the non-fluorinated analog **P1** and the reference PTA. Importantly, IR s-SNOM mapping shows that the presence of fluorine atoms in polymer **P2** improves the morphology of the polymer film, resulting in an excellent uniform coating deposited on top of the perovskite absorber layer. Thus, introducing fluorine atoms into the backbone of the $(TBT)_n$-type conjugated polymers is a promising strategy for designing new HTMs for PSCs with enhanced photovoltaic performance.

This work was supported by the Russian Science Foundation (grant no. 23-73-01196) and was partially performed employing the equipment of the Center for Collective Use of INEOS RAS.

Online Supplementary Materials

Supplementary data associated with this article can be found in the online version at doi: 10.71267/mencom.7632.

References

1 J. J. Yoo, G. Seo, M. R. Chua, T. G. Park, Y. Lu, F. Rotermund, Y.-K. Kim, C. S. Moon, N. J. Jeon, J.-P. Correa-Baena, V. Bulović, S. S. Shin, M. G. Bawendi and J. Seo, *Nature*, 2021, **590**, 587; https://doi.org/10.1038/s41586-021-03285-w.

2 G. Ren, W. Han, Y. Deng, W. Wu, Z. Li, J. Guo, H. Bao, C. Liu and W. Guo, *J. Mater. Chem. A*, 2021, **9**, 4589; https://doi.org/10.1039/D0TA11564A.

3 D. D. Astridge, J. B. Hoffman, F. Zhang, S. Y. Park, K. Zhu and A. Sellinger, *ACS Appl. Polym. Mater.*, 2021, **3**, 5578; https://doi.org/10.1021/acsapm.1c00891.

4 C. Sun, C. Zhu, L. Meng and Y. Li, *Adv. Mater.*, 2022, **34**, 2104161; https://doi.org/10.1002/adma.202104161.

5 C. Zhang, K. Wei, J. Hu, X. Cai, G. Du, J. Deng, Z. Luo, X. Zhang, Y. Wang, L. Yang and J. Zhang, *Mater. Today*, 2023, **67**, 518; https://doi.org/10.1016/j.mattod.2023.06.009.

6 S. A. Kuklin, S. V. Safronov, A. S. Peregudov, E. A. Khakina, M. M. Babaskina, M. G. Ezernitskaya, O. Yu. Fedorovskii, E. S. Kobeleva, L. V. Kulik, L. A. Frolova, P. A. Troshin and A. R. Khokhlov, *Mendeleev Commun.*, 2024, **34**, 316; https://doi.org/10.1016/j.mencom.2024.04.003.

7 E. A. Komissarova, S. A. Kuklin, A. F. Latypova, S. L. Nikitenko, V. V. Ozerova, M. N. Kevreva, N. A. Emelianov, L. A. Frolova and P. A. Troshin, *Mendeleev Commun.*, 2024, **34**, 656; https://doi.org/10.1016/j.mencom.2024.09.010.

8 N. A. Emelianov, V. V. Ozerova, A. A. Bizyaeva, M. S. Leshchev and P. A. Troshin, *Mendeleev Commun.*, 2024, **34**, 844; https://doi.org/10.1016/j.mencom.2024.10.024.

9 E. A. Komissarova, S. A. Kuklin, A. V. Maskaev, A. F. Latypova, P. M. Kuznetsov, N. A. Emelianov, S. L. Nikitenko, I. V. Martynov, I. E. Kuznetsov, A. V. Akkuratov, L. A. Frolova and P. A. Troshin, *Sustainable Energy Fuels*, 2022, **6**, 3542; https://doi.org/10.1039/D2SE00463A.

10 A. V. Akkuratov, I. E. Kuznetsov, P. M. Kuznetsov, N. V. Tukachev, I. V. Martynov, S. L. Nikitenko, A. V. Novikov, A. V. Chernyak, A. Zhugayevych and P. A. Troshin, *Synth. Met.*, 2020, **259**, 116231; https://doi.org/10.1016/j.synthmet.2019.116231.

11 A. V. Akkuratov, D. K. Susarova, L. N. Inasaridze and P. A. Troshin, *Phys. Status Solidi RRL*, 2017, **11**, 1700087; https://doi.org/10.1002/pssr.201700087.

12 W. T. Neo, K. H. Ong, T. T. Lin, S.-J. Chua and J. Xu, *J. Mater. Chem. C*, 2015, **3**, 5589; https://doi.org/10.1039/C5TC00725A.

13 C. B. Nielsen, A. J. P. White and I. McCulloch, *J. Org. Chem.*, 2015, **80**, 5045; https://doi.org/10.1021/acs.joc.5b00430.
14 N. Wang, Z. Chen, W. Wei and Z. Jiang, *J. Am. Chem. Soc.*, 2013, **135**, 17060; https://doi.org/10.1021/ja409881g.
15 N. Mallo, S. McAnally, R. Chu, M. Babazadeh, H. Jin, P. L. Burn, I. R. Gentle and P. E. Shaw, *J. Mater. Chem. C*, 2023, **11**, 14382; https://doi.org/10.1039/D3TC02740F.
16 Y. Shao, Y. Chang, S. Zhang, M. Bi, S. Liu, D. Zhang, S. Lu and Z. Kan, *Front. Chem.*, 2020, **8**, 144; https://doi.org/10.3389/fchem.2020.00144.
17 X. Gong, G. Li, C. Li, J. Zhang and Z. Bo, *J. Mater. Chem. A*, 2015, **3**, 20195; https://doi.org/10.1039/C5TA06065F.
18 C. M. Cardona, W. Li, A. E. Kaifer, D. Stockdale and G. C. Bazan, *Adv. Mater.*, 2011, **23**, 2367; https://doi.org/10.1002/adma.201004554.
19 A. F. Latypova, N. A. Emelianov, D. O. Balakirev, P. K. Sukhorukova, N. K. Kalinichenko, P. M. Kuznetsov, Y. N. Luponosov, S. M. Aldoshin, S. A. Ponomarenko, P. A. Troshin and L. A. Frolova, *ACS Appl. Energy Mater.*, 2022, **5**, 5395; https://doi.org/10.1021/acsaem.1c03119.

Received: 30th September 2024; Com. 24/7632